High-Frequency Orographically Forced variability in a Single-Layer Model of the Martian Atmosphere

Christian L. Keppenne[1,2] and Andrew P. Ingersoll[3]

[1]Jet Propulsion Laboratory
California Institute of Technology, Pasadena, CA 91109

[2]Climate Dynamics Center
University of California, Los Angeles, CA 90024

[3]Division of Geological and Planetary Sciences
California Institute of Technology, Pasadena, CA 91125

Journal of the Atmospheric Sciences, submitted
July 1993

14 double-spaced manuscript pages including cover page and figure captions
6 figures

Abstract

A shallow water model with realistic topography and idealized zonal wind forcing is used to investigate orographically forced modes in the Martian atmosphere. Locally, the model reproduces well the climatology at the sites of Viking Lander I and II (VL1 and VL2) as inferred from the Viking Lander fall and spring observations. Its variability at those sites is dominated by a 3-sol (Martian solar day) oscillation in the region of VL1 and by a 6-sol oscillation in that of VL2. These oscillations are forced by the zonal asymmetries of the Martian mountain field. It is suggested that they contribute to the observed variability by reinforcing the baroclinic oscillations with nearby periods identified in observational studies.

The spatial variability associated with the orographically forced oscillations is studied by means of extended empirical orthogonal function analysis. The 3-sol VL1 oscillation corresponds to a tropical, eastward-traveling, zonal-wavenumber one pattern. The 6-sol VL2 oscillation is characterized by two midlatitude, eastward-traveling, mixed zonal-wavenumber one and two and zonal-wavenumber three and four patterns, with respective periods near 6.1 and 5.5 sols. The corresponding phase speeds are in agreement with the conclusions drawn from the VL2 observations.

1. Introduction

In pioneering studies of the Martian atmosphere (Mintz, 1961; Leovy, 1969), baroclinic instability was recognized as the primary factor leading to the eastward-traveling waves which characterize the Martian atmosphere's synoptic variability. After the observations made by the Mariner 9 spacecraft, the Viking Lander 1 and 2 (VL1 and VL2) spacecraft revealed disturbances with periods in the range of 2-10 Martian solar days (sols). The Viking Lander observations were analyzed by Barnes (1980, 1981). With the help of the quasi-geostrophic and baroclinic instability (Charney, 1947; Eady, 1949) theories, he hypothesized the baroclinic character of the observed disturbances and determined the approximate zonal-wavenumbers associated with them. In a later paper (Barnes, 1984) the same author used quasi-geostrophic linear baroclinic models with and without a zonally symmetric topography to examine baroclinic instability in the Martian atmosphere. Zonal-wavenumber three and four disturbances were found to be the most unstable in the midlatitudes, in agreement with the conclusions inferred from the Lander data (Barnes, 1980, 1981). In the model with topography, the zonally symmetric mountain field was found to have a substantial stabilizing effect.

In the light of the above results and of observations from related studies (e.g., Leovy 1979; Pollack *et al.*, 1981), the importance of baroclinic instability in the generation of midlatitude synoptic waves is now widely recognized. In the present paper, we suggest that orographically forced waves induced by the interaction of a barotropically stable zonal flow with the zonally asymmetric component of the Martian mountain field reinforce the baroclinically unstable waves which dominate the synoptic variability. Our study is motivated by the findings of a series of papers (Legras and Ghil, 1985; Ghil, 1987; Jin and Ghil, 1990; Marcus *et al.*, 1990; Tribbia and Ghil, 1990; Strong *et al.*, 1992) in which the role played by orographically induced disturbances in the intraseasonal variability of Earth's atmosphere was elucidated. Since the ratios of the irregularities of Earth's and Mars' orographies to the scale heights of their respective atmospheres are comparable, it is likely that orographic oscillations such as those observed on Earth will also play a role in Martian meteorology.

We use a high-resolution spherical shallow water spectral model with realistic topography. Linear drag tends toward a steady zonal flow typical of equinox conditions. This idealized forcing allows us to study the role of the Martian mountain field in the generation of orographically forced waves. The model's single-layer configuration

precludes baroclinic instability - a mechanism by which zonal mean potential energy is converted to eddy potential energy in a stratified fluid - from manifesting itself. Moreover, barotropic instability - i.e. the conversion of zonal mean kinetic energy to eddy kinetic energy in the presence of an appropriate potential vorticity gradient - is also disallowed, since the zonal forcing is chosen to be barotropically stable. The model's departure from a steady state is due to the longitudinal variability of the Martian mountain field. If this variability is removed, the model evolves toward an asymptotic steady state characterized by the relaxation of the streamfunction field to the zonal forcing.

The remainder of the paper is organized as follows. The model is presented briefly in the next section, followed by a comparison of model-generated time series at the sites of VL1 and VL2 with the VL observations. The zonal structure of the variability at the VL sites is then examined by means of extended empirical orthogonal functions (EEOF) analysis. Section 4 concludes with a discussion of the results.

2. The model

We use the spectral shallow water model detailed in Keppenne (1992). The dimensionless system of prognostic equations is:

$$\partial_t \Delta\psi = -\nabla.[\,\mathbf{u}(\Delta\psi + f)] - \tau U \Delta\psi + (-)^{n+1}\gamma \Delta^n \psi - \varepsilon \Delta(\psi - \psi^*) \quad , \qquad (1a)$$

$$\partial_t \Delta\chi = \mathbf{k}.\nabla\times[\,\mathbf{u}(\Delta\psi + f)] - \tau U \Delta\chi + (-)^{n+1}\gamma \Delta^n \chi - \Delta\left[\frac{\mathbf{u}.\mathbf{u}}{2} + \phi\right] \quad , \qquad (1b)$$

$$\partial_t \phi = -\nabla.[\mathbf{u}(\phi - \phi_b)] - (\varphi - \varphi_b)\Delta\chi \qquad (1c)$$

(1a-b) is the vorticity-divergence form of the momentum equation and (1c) is the mass conservation equation. $\psi((\lambda, \theta, t)$, $\chi(\lambda, \theta, t)$, and $\phi(\lambda, \theta, t)$, are the streamfunction, velocity potential, and the deviation of the geopotential height of the free surface $h(\lambda, \theta, t)$, representing the top of the atmosphere, from its global average φ, so that $\phi+\varphi = gh$, where g is the acceleration of gravity. λ is longitude, θ latitude, and t time. The dimensionless time unit is equal to the Martian rotation period $2\pi/\Omega$ and the dimensionless length unit is R, the equatorial radius of Mars. $\mathbf{u}(\lambda, \theta, t)$ is the horizontal fluid velocity, $f=2\Omega sin\theta$ is the Coriolis parameter, τ is a drag coefficient, γ is a diffusion coefficient, U is the instantaneous global mean square-root zonal kinetic energy per unit mass, ϕ_b (λ, θ) is topography and $\Delta$is the Laplacian operator.

The relaxation term, $\varepsilon \Delta (\psi - \psi^*)$, is applied only to the spectral coefficients corresponding to zonal spherical harmonics. The forcing $\psi^*(\theta)$ corresponds to a forcing wind field, $u^*(\theta) = -\partial\psi^*(\theta)/\partial\theta$, which has a midlatitude jet of $30\ ms^{-1}$ and is symmetric about the equator to account for the effect of equinoctial solar heating on the Martian circulation. When the longitudinal variability of the mountain field is ignored, this forcing field and the model's response to it satisfy the criterion for barotropic stability (e.g., Pedlosky, 1987): the poleward gradient of the absolute vorticity, $\Delta\psi+f$, does not change sign anywhere between the poles. However, the model's response to ψ^* becomes unsteady when the longitudinal variations of the Martian orography are accounted for, leading to the variability discussed in the following sections.

The free surface of the shallow water layer is representative of the 2 mb pressure level ($\varphi - \varphi_b = 30 = gh\ (2\pi/\Omega)^2 / R^2$, $h = 30\ R^2\ sol^{-2} / g \sim 13\ km$ in (1c)). τ is 0.1 and the drag terms in (1a-b) are applied selectively to the spectral coefficients corresponding to nonzonal spherical harmonics. The relaxation time, $1/\varepsilon$, is 10 sols. $n = 4$ in (1a-b) to selectively damp high-wavenumber oscillations, and γ, the diffusion coefficient, is $5\ 10^{-12}$. As a result, a wavenumber-20 disturbance will damp with a time constant of approximately 6 days.

The spectral form of (1) is integrated at rhomboidal truncation R20 using an associated Gaussian grid with 50 Gaussian latitudes and 64 meridians and a realistic mountain field interpolated from the topography of Pollack *et al.*'s (1990) Martian GCM. The transform method (Orszag, 1970; Eliassen *et al.*, 1970; Bourke, 1972) is used to iterate back and forth between the gridpoint and spectral representations of the model variables.

3. Results

The model was run for 6000 sols from the initial condition of an atmosphere at rest ($\psi = \chi = \phi = 0$) and the first 1000 sols of model history were discarded to eliminate undesired transients. Fig. 1 gives a global picture of the variability during the last 5000 sols of the run by showing the spatial distribution of $f_m(\lambda, \theta)$, the frequency associated with the highest power spectral density of the geopotential field. The geopotential variable is directly proportional to pressure in this model.

[Fig. 1 near here, please]

While the power spectra of global model quantities such as its integrated atmospheric angular momentum have most of their power associated with low frequencies around 1/100 $sols^{-1}$ (Keppenne, 1992), the local time series are dominated by much higher-frequency oscillations with periods in the range of 2.5-10 sol. f_m is 1/3.6 sol^{-1} at the location of VL1 (22º N, 48º W) and 1/6.0 sol^{-1} at the VL2 site (48º N, 134º E). These results are consistent with the springtime VL observations. Also consistent with the observations are the ratios $\sigma_\phi / (\varphi - \varphi_b)$ of the geopotential standard deviation to the modeled depth of the Martian atmosphere. These are 0.009 and 0.015, respectively at the sites of VL1 and VL2. The corresponding ratios are 0.008 and 0.016 for the pressure observations in the Fall season, and 0.0065 and 0.019 for the Spring observations. In other words, the model's orographically forced variance is comparable to the observed variance.

One interesting feature of Fig. 1 is that f_m is not a continuous function of location. Rather, Fig. 1 has a number of plateaus separated by abrupt variations. This behavior is typical of orographically forced waves (e.g., Gill, 1982) and the zonally asymmetric distribution of f_m is a sign that the corresponding variability is induced by the mountain field. Indeed, if it were not for the zonally asymmetric topography, the time-independent model statistics would have a zonal distribution reflecting the zonal symmetry of the forcing.

Fig. 2 shows power spectra of the geopotential variable at the sites of VL1 and VL2. These power spectra are computed by the maximum entropy method for spectral estimation (MESA: Yule, 1927; Walker, 1931; Burg, 1968) using Burg's (1968) algorithm. 60 poles are used in the computations. The geopotential power spectrum at VL1 (Fig. 2a) shows a pronounced peak centered at a frequency of 0.28 $sols^{-1}$. The corresponding period of 3.6 sols is close to the 3.7-sol period which dominates the VL1 fall pressure observations (Barnes, 1980), and not too distant from the 3.0-sol period which corresponds to the most pronounced feature of the spring observations at the same site. The model variability in the region of VL2 is dominated by a 6-sol oscillation whose signature is the most striking feature of Fig. 2b. This result is also consistent with the VL2 pressure observations: Barnes (1980) reports a very distinct peak corresponding to a period of 6.7 sols in the

power spectrum of the VL2 pressure during the fall season, and another with an associated period of 8 sols in the springtime observations at the same location.

[Fig. 2 near here, please]

The power spectral density associated with the 3.6-sol model oscillation at VL1 is about one order of magnitude less than that corresponding to the 6.0-sol oscillation at VL2. The same relationship exists between the power spectral densities associated with the observed 3.7-sol and 6.7-sol oscillations in the VL1 and VL2 pressure data (Barnes, 1980). However, the power spectra of the model variables show much narrower peaks than those corresponding to the observations. The most probable explanation is that although the model captures the part of the variability that is orographically forced, it does not reproduce the fraction that is induced by baroclinic instability. In the Martian atmosphere, the orographic forcing should reinforce the observed baroclinic oscillations. The 3.6-sol and 6.0-sol oscillations it produces may explain why most of the observed power is found near the corresponding frequencies. The model has more of its power at low frequencies than the observations have.

The similarities between the model results and Barnes' (1980) observations extend to the phase lag between pressure and meridional velocity and to the meridional fluxes of zonal momentum and pressure: v leads ϕ by about 80° near VL2, in the model as in the observations, and - using primes to denote anomalies and angle brackets to indicate time averaging - $\langle u'v' \rangle$ is positive at both VL sites. Also in agreement with the observations, $\langle v'\phi' \rangle$ is negative. However, although these phase lag and fluxes correspond to what would be expected from a baroclinically unstable zonal jet, their cause in our single-layer model must lay in the interaction of the flow with the Martian orography.

To analyze the longitudinal character of the 3.6-sol and 6.0-sol orographically forced oscillations identified at the VL sites, EEOF decomposition (e.g., Weare and Nasstrom, 1982; Lau and Chan, 1986; Graham et al., 1987a,b) is applied to multivariate time series of geopotential anomaly at the corresponding latitudes. EEOF analysis is a variant of principal component analysis (PCA: e.g., Preisendorfer, 1988) applied simultaneously in the temporal and spatial domains. The algorithm provides the basis vectors of a new coordinate system, the EEOFs, and the corresponding principal components (PCs) which give the representation of the model's trajectory in the new coordinate system. The main advantage of the EEOFs as basis vectors is that they are data-adaptive and indicate the directions of phase space along which

the variability of the model's trajectory is maximum (e.g., Mo and Ghil, 1987; Ghil, 1988). The data-adaptive character of the method makes it possible to distinguish between oscillations of nearby periods whose signatures are blurred into a single peak in the power spectra of Fig. 2.

EEOF analysis is applied to the geopotential anomaly at the latitude of VL2 with a time window of 10 sols. The resulting singular spectrum contains two pairs of singular values (SVs) of nearly equal size. Such pairs have a particular significance in that they isolate an anharmonic oscillation from the remaining variability and noise (Vautard and Ghil, 1989). The EEOFs associated with those pairs isolate 13.2% and 7.6% of the total variance, respectively. The MESA spectra of their respective PCs are shown in Fig. 3. The first pair (PCs 3-4) carries a 6.1-sol oscillation, while the second pair (PCs 8-9) oscillates with a period of 5.5 sols. The 6.0-sol variability observed in the model geopotential at VL2 can be understood as a combination of the two oscillations carried by the two pairs of EEOFs and PCs observed at this latitude.

[Fig. 3 near here, please]

Fig. 4 shows time-longitude diagrams of EEOFs 3-4 and 8-9. Like the corresponding PCs, the two EEOFs of each pair are in quadrature, as can be expected from pairs of EOFs and PCs carrying a same oscillation (Vautard and Ghil, 1989). Fig. 6a-b show an eastward-propagating mixed zonal-wavenumber one and two pattern. The phase speed associated with this pattern is about 17 m s^{-1}. The mixed zonal-wavenumber three and four pattern in Fig. 6c-d also propagates eastward, this time at about half the other pattern's speed. These phase speeds are in the range of phase speeds estimated by Barnes (1980) from the VL observations.

[Fig. 4 near here, please]

When EEOF analysis is applied with the same time window to the geopotential anomaly at the latitude of VL1, the method isolates one pair of singular values of nearly equal size. This pair (SVs 3-4) carries 9.2% of the variability at that latitude. The MESA spectra of the corresponding PCs, shown in Fig. 5, reveal a single peak at a frequency of 1/3.2 sol^{-1}. Fig. 1 shows that this frequency dominates the variability east of VL1. Fig. 6 shows the associated EEOFs. They isolate an eastward-traveling zonal-wavenumber one pattern. This pattern travels much faster than the midlatitude oscillations discussed in the previous paragraph. It

revolves around the globe at 55 m s^{-1}. The lack of observational data provided by VL1 does not allow the reliable calculation of an observed phase speed for comparison purposes.

[Figs. 5 and 6 near here, please]

4. Discussion

The model results suggest that orographically forced oscillations with periods near 3.6 and 6.0 sols play a role in determining the Martian atmosphere's 1.0-10.0 sol variability at the sites of VL1 and VL2 by reinforcing the baroclinically unstable modes with nearby periods detected in Barnes (1980, 1981) studies. Since the model's single-layer configuration prevents the manifestation of baroclinic waves, and since its response to the equinoctial zonal forcing is barotropically stable if the longitudinal variability of the Martian mountain field is ignored, we concluded that the orographically forced modes are induced by the interaction of the zonal flow with this longitudinal variability.

Although the model's orographically forced variance is comparable to the observed pressure variance, it is still unclear what fraction of the observed variability near 3.6 sols and 6.0 sols is caused by orographically forced oscillations such as those identified in the present study. The power spectra of Figs. 2, 3 and 5 suggest that this fraction may be fairly small, since their peaks are sharper, narrower, and involve less total power than those associated with nearby-period oscillations in the VL observations. The model has more of its power at low frequencies than do the observations. A similar analysis with a multi-layer version of the model would help answer this question by revealing how much more power is concentrated near these periods when baroclinic instability is allowed to occur. We feel that the most significant result of the present study is the manifestation of the orographically forced modes at periods close to the ones observed in the VL data. Since earlier studies have shown that the range of observed periods and zonal wavenumbers are baroclinically unstable, the reinforcement of the near-3.0-sol and near-6.0-sol instabilities, respectively at VL1 and VL2, may explain why these particular periods are the most excited among the whole range of unstable modes predicted by baroclinic theory (e.g., Barnes, 1984, 1986).

Acknowledgment

The authors acknowledge interesting conversations with D.J. Banfield, D.H. Boggs, J.O. Dickey, M. Ghil and S.L. Marcus. They also thank Jim Pollack for providing the Martian GCM topography and an anonymous referee of an earlier version of this paper for his constructive criticisms and suggestions.

The research described in this publication was carried out in part by the Jet Propulsion Laboratory (JPL), California Institute of Technology (CIT), under a contract with the National Aeronautics and Space Administration and in part by the Climate Dynamics Center, University of California, Los Angeles. It was funded through the JPL/CIT Director's Discretionary Fund for 1992. The model development and simulations took place on JPL's and the NASA Ames Research Center's CRAY Y-MP computers.

References

Barnes, J.R., 1980: Time spectral analysis of midlatitude disturbances in the Martian atmosphere, *J. Atmos. Sci.*, 37, 2002-2015.

Barnes, J.R., 1981: Midlatitude disturbances in the Martian atmosphere: a second Mars year, *J. Atmos. Sci.*, 38, 225-234.

Barnes, J.R., 1984: Linear baroclinic instability in the Martian atmosphere, *J. Atmos. Sci.*, 41, 1536-1550.

Barnes, J.R., 1986: Finite amplitude behavior of a single baroclinic wave with multiple vertical modes: effects of thermal damping, *J. Atmos. Sci.*, 43, 58-71.

Bourke, W., 1972: An efficient, one-level, primitive-equation spectral model, *Mon. Wea. Rev.*, 100, 683-689.

Burg, J., 1968: Maximum entropy spectral analysis, Presentation at 37th annual meeting of the Society of Exploratory Geophysicists, Oklahoma City, 1967, reprinted in *Modern Spectrum Analysis*, D. G. Childers (ed.), pp.34-48.

Charney, J.G., 1947: The dynamics of long-waves in a baroclinic westerly current, *J. Meteor.*, 4, 135-162.

Eady, E.T., 1949: Long waves and cyclone waves, *Tellus*, 1, 33-52.

Eliassen, E., B. Machenhauer, and E. Rassmusen, 1970: On a numerical method for integration of the hydrodynamical equations with spectral representation of the horizontal fields, Rept. 2, Institute for Theoretical Meteorology, University of Copenhagen, 35pp.

Gill, A.E., 1982: *Atmosphere Ocean Dynamics*, Academic Press, New York, 664pp.

Ghil, M., 1987: Dynamics, statistics and predictability of planetary flow regimes, in *Irreversible Phenomena and Dynamical Systems Analysis in Geosciences*, C. and G. Nicolis (eds.), Reidel, Boston, pp. 241-283.

Ghil, M., Nonlinear approaches to low-frequency atmospheric variability. in *Dynamics of Low-Frequency Phenomena in the Atmosphere*, G. Branstator *et al.* (Eds.), National Center for Atmospheric Research, Boulder, Colorado, pp.603-714, 1988.

Golub and Van Loon, 1989: *Matrix Computations*, Johns Hopkins University Press, Baltimore, MD, 642pp.

Graham, N. E., J. Michaelsen, and T. P. Barnett, 1987a: An investigation of the El Niño-Southern Oscillation cycle with statistical models - 1. Predictor field characteristics, *J. Geophys. Res.*, 92, 14251-14270.

Graham, N. E., J. Michaelsen, and T. P. Barnett, 1987b: An investigation of the El Niño-Southern Oscillation cycle with statistical models - 2. Model results, *J. Geophys. Res.*, 92, 14271-14289.

Jin, F-f., and M. Ghil, 1990: Intraseasonal oscillations in the extratropics: Hopf bifurcation and topographic instabilities, *J. Atmos. Sci.*, **47**, 823-839.

Keppenne, C.L., 1992: Orographically forced oscillations in a dynamical model of the Martian atmosphere, *Icarus*, 100, 598-607.

Lau, K.M., and P.H. Chan, 1986: Aspects of the 40-50 day oscillation during the northern summer as inferred from outgoing longwave radiation, *Mon. Wea. Rev.*, **114**, 1354-1367.

Legras, B., and M. Ghil, 1985: Persistent anomalies, blocking and variations in atmospheric predictability, *J. Atmos. Sci.*, **43**, 433-471.

Leovy, C.B., 1969: Mars: theoretical aspects of meteorology, *Appl. Opt.*, **8**, 1279-1286.

Leovy, C.B., 1979: Martian meteorology, Ann. Rev. Astron. Astrophys., **17**, 387-413.

Marcus, S., M. Ghil, J. Dickey, and T. Eubanks, 1990: Origin of the 30-60 day oscillation in the length of day and atmospheric angular momentum,: new findings from the UCLA general circulation model, in *Earth Rotation and Reference Frames for Geodesy and Geodynamics*, G. A. Wilkins (ed.), pp. 98-105, Springer-Verlag, New York.

Mintz, Y., 1961: The general circulation of planetary atmospheres, in *The Atmospheres of Mars and Venus*, NAS-NRC, Publ. 944, 107-146.

Mo, K.C., and M. Ghil, Statistics and dynamics of persistent anomalies, *J. Atmos. Sci.*, **44**, 877-901, 1987.

Orszag, S., 1970: Transform method for the calculation of vector-coupled sums: application to the spectral form of the vorticity equation, *J. Atmos. Sci.*, **27**, 890-895.

Pedloski, J, 1987: *Geophysical Fluid Dynamics*, 2nd ed., Springer Verlag, New York, 710pp.

Pollack, J., C. Leovy, P. Greiman, and Y. Mintz, 1981: A Martian general circulation experiment with large topography, *J. Atmos. Sci.*, 38, 3-29.

Pollack, J., R. Haberle, J. Schaeffer, and H. Lee, 1990: Simulation of the general circulation of the Martian atmosphere: I - polar processes, *J. Geophys. Res.*, **95**, 1447-1474.

Preisendorfer, R.W., 1988: *Principal Component Analysis in Meteorology and Oceanography*, C.D. Mobley (Ed.), Elsevier, Amsterdam, 425pp.

Strong, C., F-f. Jin, and M. Ghil, 1992: Intraseasonal oscillations and the stability of a seasonally-forced barotropic model, in *Proceedings of the XVIIth Annual Climate Diagnostics Workshop*, Climate Analysis Center, National Meteorological Center, National Oceans and Atmosphere Administration.

Tribbia, J., and M. Ghil, 1990: Forced zonal flow over topography and the 30-60 day oscillation in atmospheric angular momentum, NCAR 0501/89-5, 26pp., National Center for Atmospheric Research, Boulder, Co.

Vautard, R., and M. Ghil, 1989: Singular spectrum analysis in nonlinear dynamics, with applications to paleoclimatic time series, *Physica D*, **35**, 395-424.

Walker, G., 1931: On periodicity in series of related terms, *Proc. R. Soc. Lond.*, **A 131**, 518-532.

Weare, B.C., and J.S. Nasstrom, 1982: Examples of extended empirical orthogonal function analyses, *Mon. Wea. Rev.*, **110**, 481-485.

Yule, G., 1927: On a method of investigating periodicities in disturbed series, *Phil. Trans. R. Soc. Lond.*, **A 226**, 267-298.

Captions to figures

Fig. 1. Geographical distribution of *fm*, the frequency associated with the highest power spectral density of the model's geopotential field. The horizontal axes show the colatitude and longitude in degrees and *fm* is expressed in cycles/sol.

Fig. 2. Power spectra of local geopotential time series at the sites of (a and b) Viking Lander 1 and 2 (VL1 and VL2). The frequency scales are logarithmic and in units of sol^{-1}. The power spectral densities are multiplied by frequency. Thus, the labels along the vertical axes are in units of m^2.

Fig. 3. Power spectra of (a) principal components (PCs) 3-4 and (b) PCs 8-9 resulting from the extended empirical orthogonal function (EEOF) decomposition of the geopotential history at the latitude (48ºN) of VL2. As in Fig. 2, the frequency axes are labeled in sol^{-1}. The power spectral densities are multiplied by frequency and the vertical units are dimensionless because the PCs have been normalized to unity. The solid (dashed) lines show the power spectra corresponding to the lower-order (higher-order) PC of each pair.

Fig. 4. Time-longitude diagrams of EEOFs (a-b) 3-4 and (c-d) 8-9 resulting from the EEOF decomposition of the geopotential history at the latitude of VL2. The horizontal and vertical axes respectively indicate the longitude in degrees and the time dimension of the EEOFs in sols.

Fig. 5. Same as Fig. 3 for PCs 3-4 resulting from the EEOF decomposition of the geopotential history at the latitude of VL1.

Fig. 6. Same as Fig. 4 for EEOFs (a-b) 3-4 resulting from the EEOF decomposition of the geopotential history at the latitude of VL1.

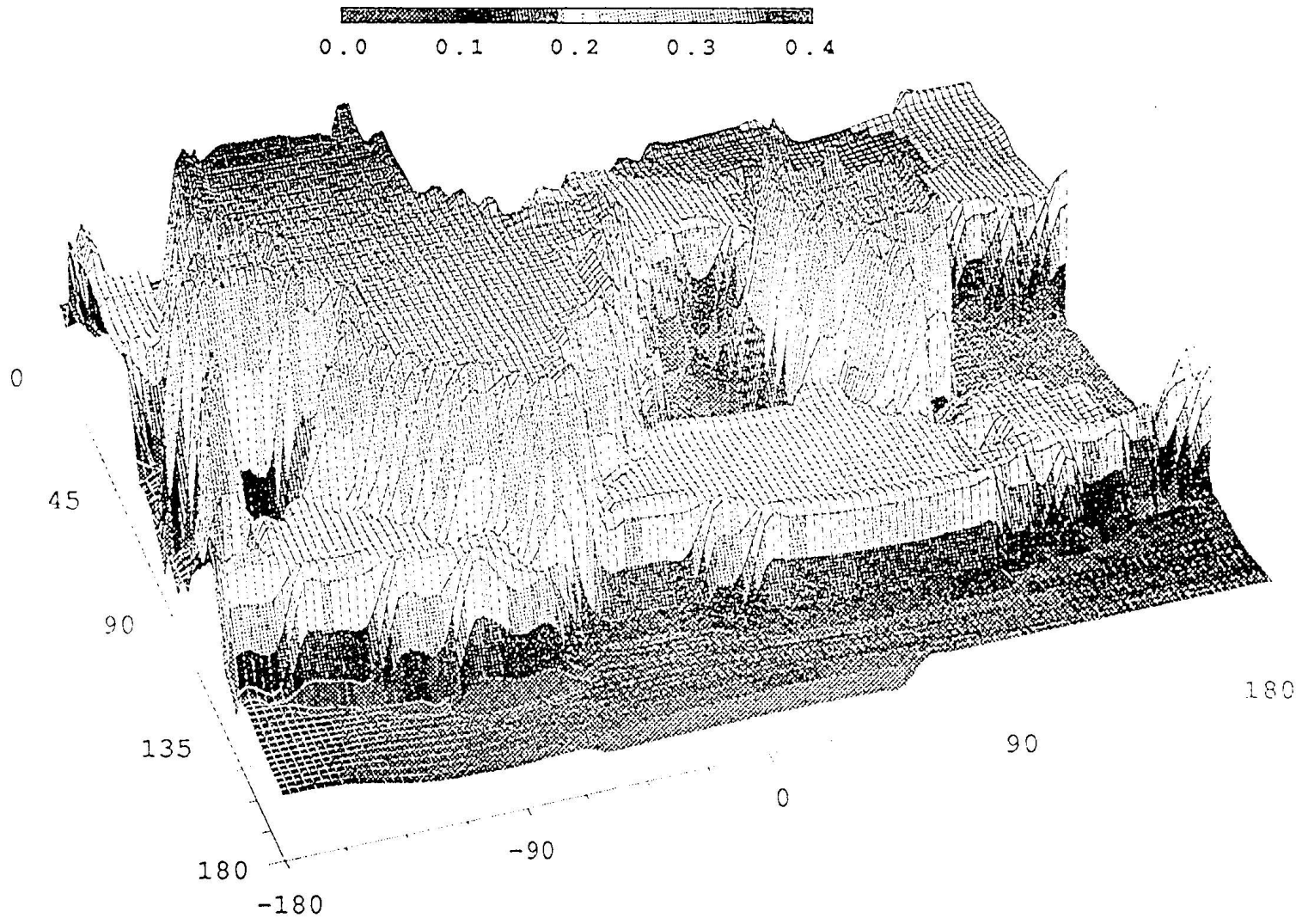

Christian L.Keppenne and Andrew P. Ingersoll - Figure 1

(a)

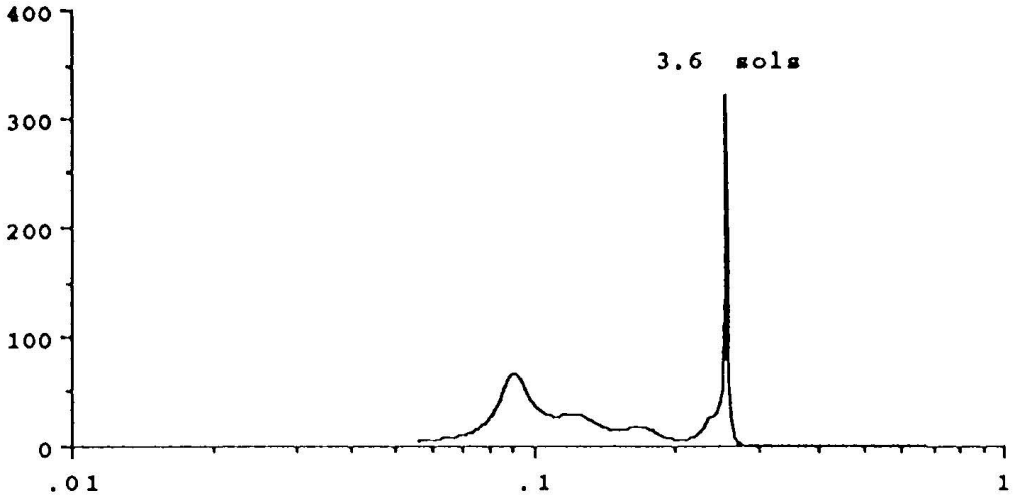

(b)

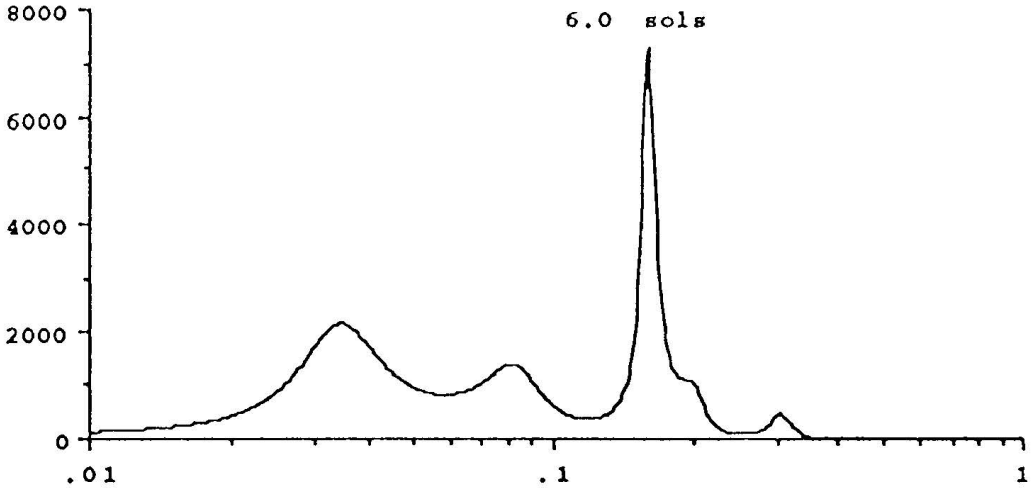

Christian L. Keppenne and Andrew P. Ingersoll - Figure 2

(a)

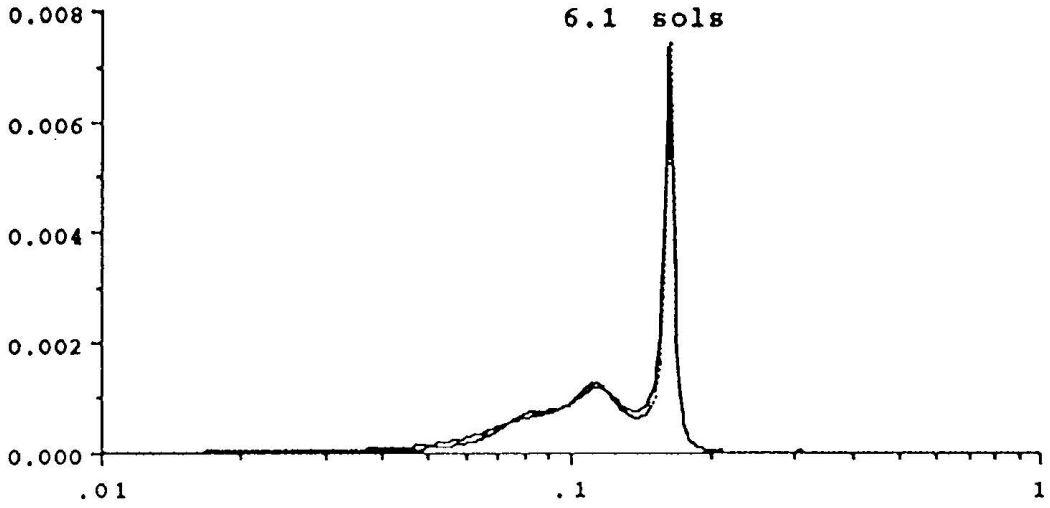

(b)

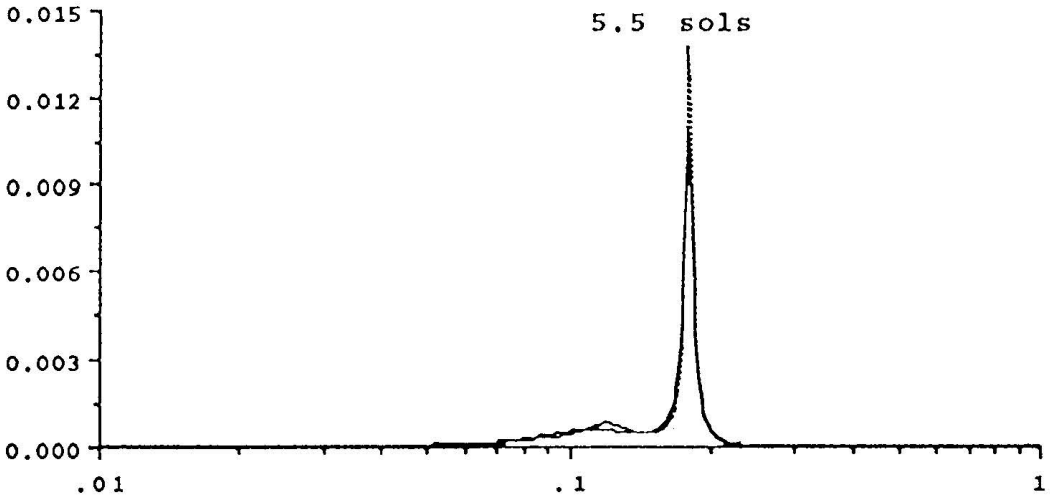

Christian L. Keppenne and Andrew P. Ingersoll - Figure 3

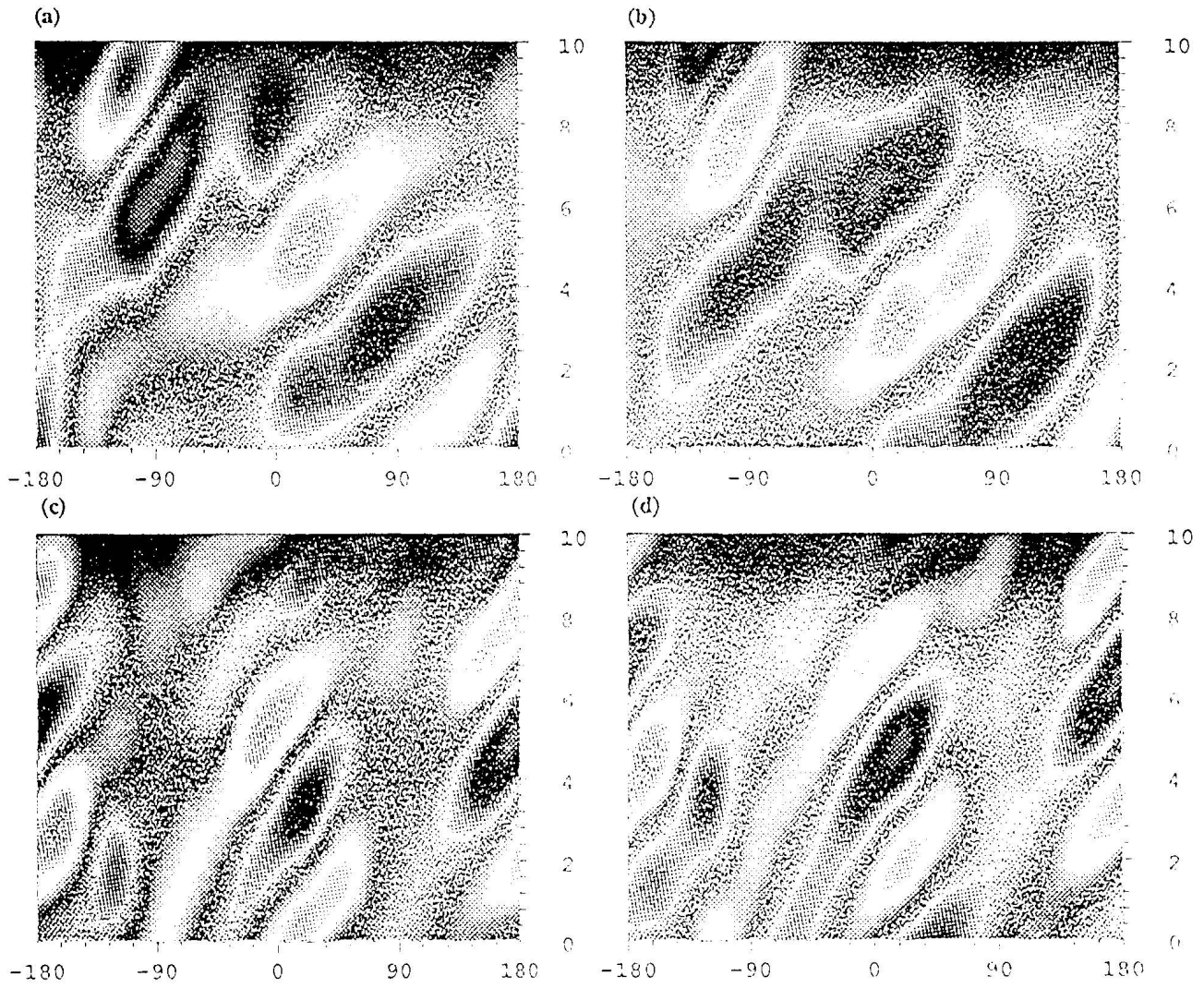

Christian L. Keppenne and Andrew P. Ingersoll - Figure 4

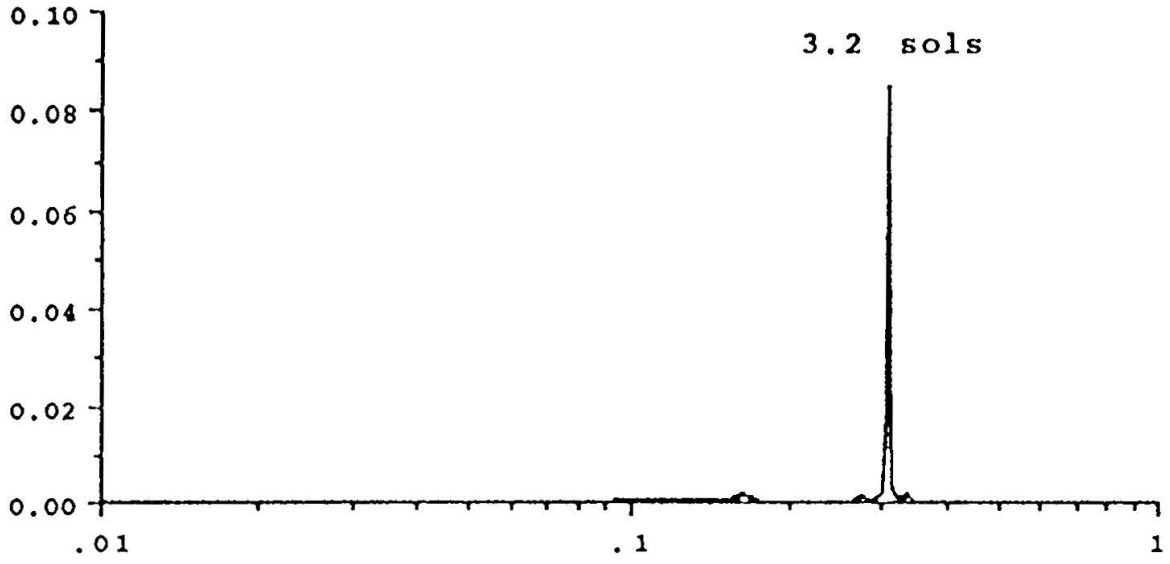

Christian L. Keppenne and Andrew P. ingersoll - Figure 5

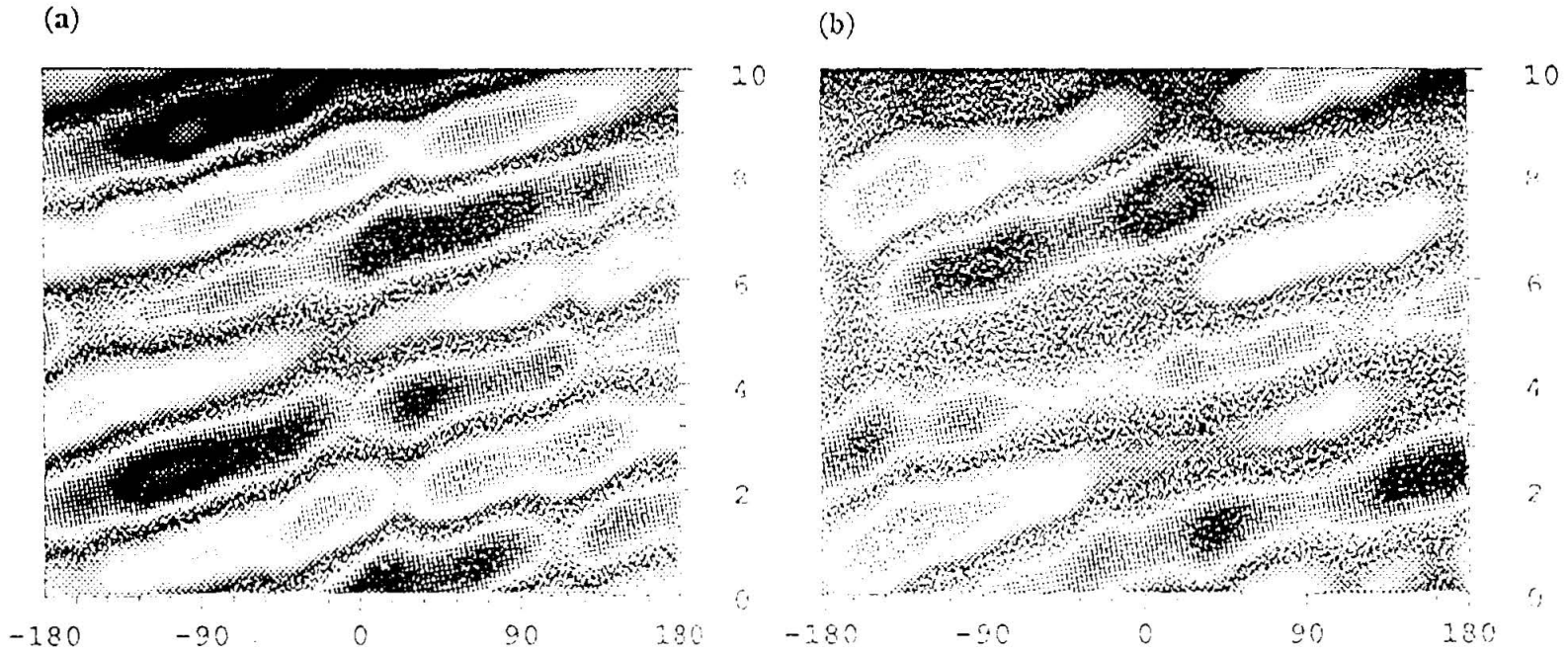

Christian L. Keppenne and Andrew P. Ingersoll - Figure 6